Highly Stable Photoelectrochemical Water Splitting and Hydrogen Generation Using a Double-Band InGaN/GaN Core/Shell Nanowire Photoanode

ARTICLE *in* NANO LETTERS · AUGUST 2013

Impact Factor: 13.59 · DOI: 10.1021/nl402156e · Source: PubMed

6 AUTHORS, INCLUDING:

Bandar AlOtaibi
McGill University
14 PUBLICATIONS **66** CITATIONS
SEE PROFILE

Hieu Nguyen
New Jersey Institute of Technology
64 PUBLICATIONS **537** CITATIONS
SEE PROFILE

Sammy Zhao
Harbin Engineering University
27 PUBLICATIONS **264** CITATIONS
SEE PROFILE

Md Golam Kibria
McGill University
32 PUBLICATIONS **443** CITATIONS
SEE PROFILE

NANO LETTERS

Letter

pubs.acs.org/NanoLett

Highly Stable Photoelectrochemical Water Splitting and Hydrogen Generation Using a Double-Band InGaN/GaN Core/Shell Nanowire Photoanode

B. AlOtaibi, H. P. T. Nguyen, S. Zhao, M. G. Kibria, S. Fan, and Z. Mi*

Department of Electrical and Computer Engineering, McGill University, 3480 University Street, Montreal, Quebec H3A 0E9, Canada

Supporting Information

ABSTRACT: We report on the first demonstration of stable photoelectrochemical water splitting and hydrogen generation on a double-band photoanode in acidic solution (hydrogen bromide), which is achieved by InGaN/GaN core/shell nanowire arrays grown on Si substrate using catalyst-free molecular beam epitaxy. The nanowires are doped n-type using Si to reduce the surface depletion region and increase current conduction. Relatively high incident-photon-to-current-conversion efficiency (up to ~27%) is measured under ultraviolet and visible light irradiation. Under simulated sunlight illumination, steady evolution of molecular hydrogen is further demonstrated.

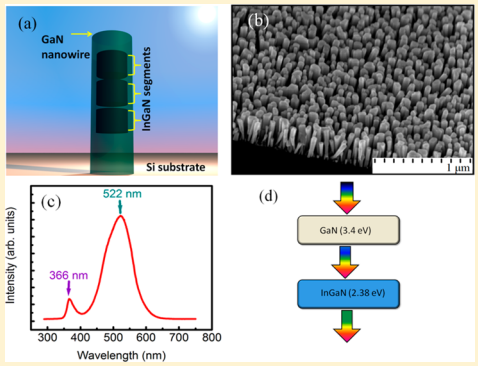

KEYWORDS: *Nanowire, InGaN, photoelectrochemical water splitting, hydrogen, solar fuels*

The effective capture of sunlight and subsequent conversion into chemical fuels such as hydrogen has attracted considerable attention.[1−6] Compared to solar electricity, the use of chemical bonds to store solar energy promises significantly reduced device fabrication cost, as well as the cost associated with energy storage.[7,8] In this regard, hydrogen production by photoelectrolysis of water with semiconductor materials offers a clean, environmentally friendly process.[7−9] In this process, solar energy is used to convert water into hydrogen and oxygen

$$H_2O + 1.23\ eV \rightarrow H_2 + \tfrac{1}{2}O_2 \quad (1)$$

Critical for the realization of a practical, complete solar fuel system are highly efficient, paired photoanodes and photocathodes. It is essential that the photoelectrodes are stable against corrosion and oxidation, particularly in acidic solutions. While relatively efficient and stable photocathodes, including p-InP and Si, have been demonstrated,[10,11] a stable photoanode that can operate in acidic media has remained elusive. For example, the commonly reported metal oxide electrodes are only stable in alkaline solutions. In addition, due to the large bandgap, their energy conversion efficiency is extremely low under direct solar irradiation.[12−16] Various schemes for narrowing the energy bandgap of oxide semiconductors and for protecting the surface from oxidization and corrosion have been explored but with limited success.[17−22] Additionally, multijunction photoelectrodes have been investigated to improve the solar-to-hydrogen conversion efficiency.[4,23,24] However, the integration of dissimilar materials often limits the performance, reliability, and scalability.

In this regard, metal-nitride semiconductors have emerged as a new class of materials for photoelectrochemical water splitting and hydrogen production.[25−27] The energy bandgap of $In_xGa_{1-x}N$ can be tuned to cover nearly the entire solar spectrum,[28] thereby promising multiband solar-to-hydrogen conversion devices using a single alloy material. Uniquely, the band edges of InGaN can straddle with hydrogen reduction and water oxidation for up to nearly the bandgap of 1.23 eV, which is thermodynamically required to split water.[29] Recently, the photoelectrochemical properties of metal nitrides have been investigated. With the use of nanowire structures, the energy conversion efficiency can be further improved due to the reduced defect densities and enhanced charge separation, compared to previously reported planar structures.[27,30−32] To date, however, there have been no reports on the direct measurements of photoelectrochemical hydrogen generation using InGaN nanowire photoelectrodes under visible light irradiation. Moreover, the stability of such nanostructured electrodes against photocorrosion has also remained unknown.

Here, we have investigated photoelectrochemical water splitting by using a core−shell InGaN/GaN nanowire photoanode in acidic solution (HBr) under ultraviolet (UV) and visible light irradiation. We have demonstrated for the first time stable hydrogen production on InGaN nanowire photoelectrode. Such unique core−shell structures can function effectively as a double-band photoelectrode, leading to relatively high incident-photon-

Received: June 13, 2013
Revised: July 28, 2013
Published: August 6, 2013

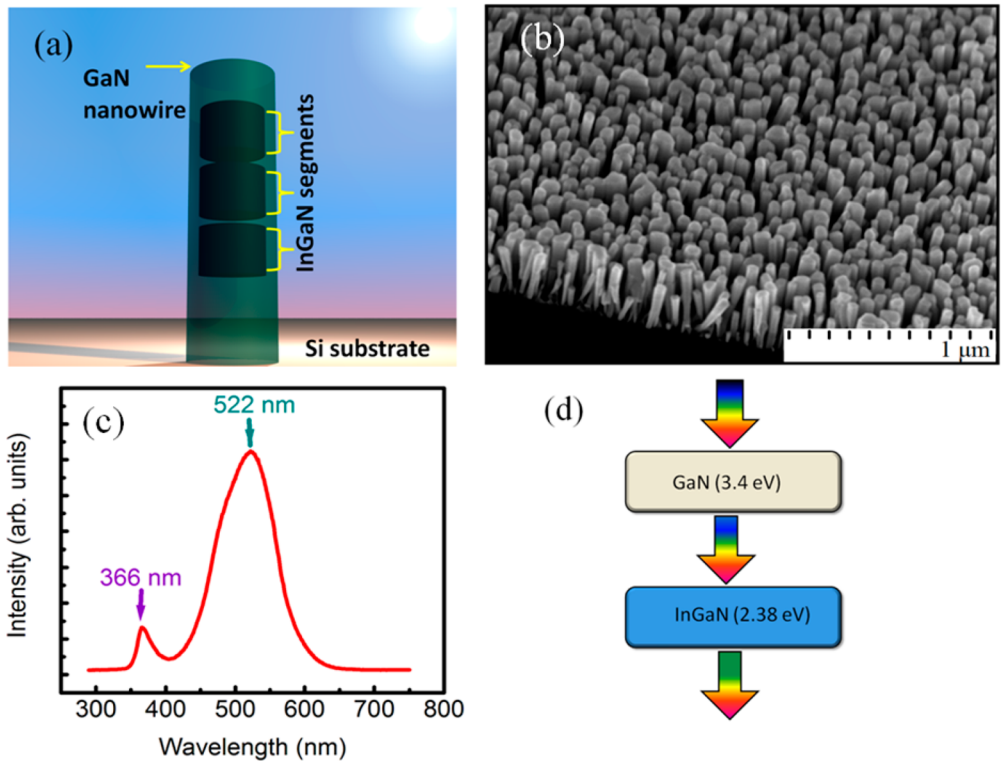

Figure 1. (a) Schematic of InGaN/GaN core/shell nanowire structures. (b) SEM image of InGaN/GaN core/shell nanowire arrays grown on Si(111) substrate. (c) Photoluminescence spectrum of InGaN/GaN core−shell nanowires. (d) Schematic of double-band photoelectrode concept.

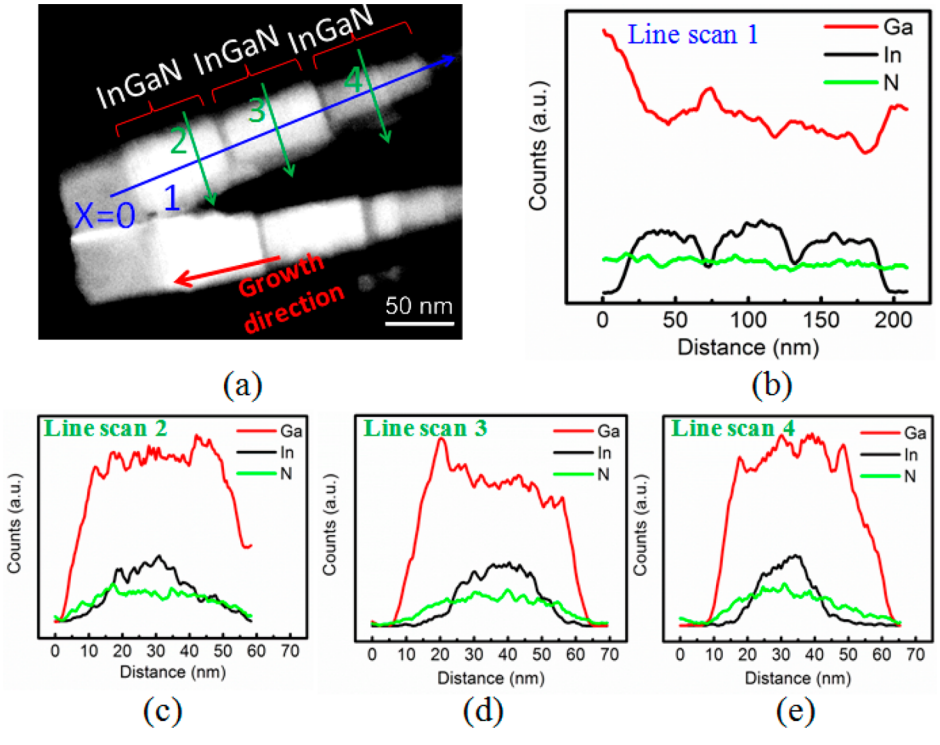

Figure 2. (a) HAADF showing three InGaN segments embedded in a GaN nanowire. (b−e) EDX line scans showing the distribution of In, Ga and N along the lines (1−4) in (a).

to-current-conversion efficiency (IPCE) (up to ~27%). Detailed studies further confirm that the InGaN/GaN core−shell nanowire photoanode shows virtually no degradation after an extended period of reaction in HBr, which is attributed to the controlled surface polarity of the nearly dislocation-free nanowire structures as well as the presence of intrinsic surface states near the band edges, rather than the center of the bandgap, due to the strong ionic character of III-nitrides.[33,34] In addition, the thin GaN shell can further protect the InGaN segment from corrosion and oxidation.

dx.doi.org/10.1021/nl402156e | *Nano Lett.* 2013, 13, 4356−4361

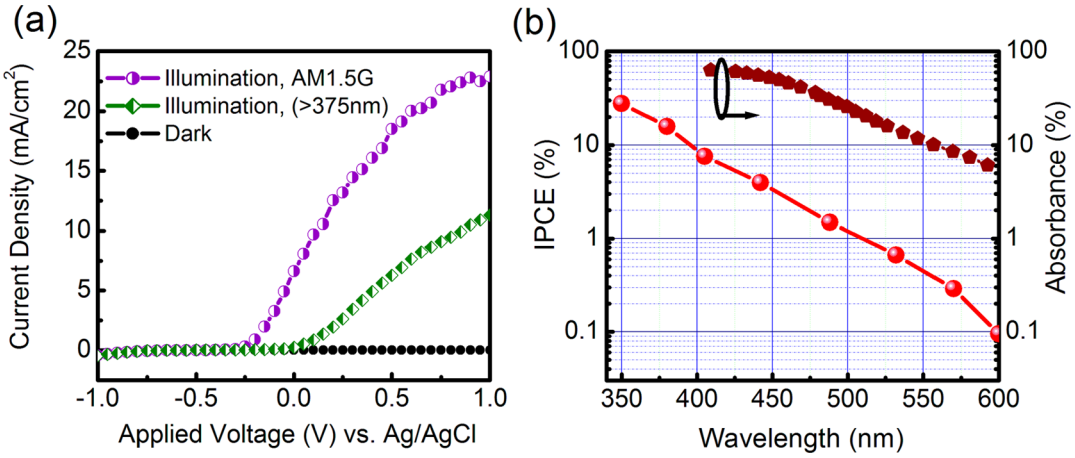

Figure 3. (a) Variations of the current density with applied voltage (vs Ag/AgCl) in 1 mol/L HBr under simulated sunlight illumination. The response from InGaN nanowires is clearly confirmed with the use of a long-pass (>375 nm) filter. The measured current density is ~23 mA/cm^2 using a 300W Xe lamp with AM1.5G filter at a bias of 1 V (vs Ag/AgCl). (b) Incident-photon-to-current conversion efficiency (IPCE) of InGaN/GaN nanowire photoelectrodes measured at an applied bias of 1 V (vs Ag/AgCl) in 1 mol/L HBr in log scale. The calculated spectral absorbance by the InGaN segments is also shown for comparison.

Catalyst-free, vertically aligned InGaN/GaN core/shell nanowire arrays, schematically shown in Figure 1a, were grown on n-type Si(111) substrate by radio frequency plasma-assisted molecular beam epitaxy under nitrogen rich conditions. After an in situ oxide desorption at ~770 °C, a GaN nanowire template with a height of ~200 nm was first grown on Si(111) substrate. The use of GaN nanowire template instead of the direct formation of InGaN nanowires on Si can lead to nanowire structures with controlled structural and optical properties. Subsequently, three InGaN(70 nm)/GaN(10 nm) segments were grown at a reduced substrate temperature of ~600 °C to enhance In incorporation. Because of the preferential In desorption from the lateral surfaces, unique core−shell structures, illustrated in Figure 1a, are formed during the growth process. The In composition can be controlled by varying the In/Ga flux ratios and/or the substrate temperature. Other growth parameters include a nitrogen flow rate of ~1 sccm and plasma forward power of ~350 W.[35,36] The nanowires are doped n-type using Si to reduce the surface depletion region and enhance the current conduction. Shown in Figure 1b is the scanning electron microscopy (SEM) image of InGaN/GaN nanowire arrays on Si. The wires are nearly vertically aligned to the substrate with their sidewalls being the nonpolar plane. The wire lengths and diameters are in the ranges of 400−500 nm and 80−140 nm, respectively. Optical properties of InGaN/GaN nanowire arrays were further studied by photoluminescence spectroscopy. Illustrated in Figure 1c, the emission peaks at ~366 and 522 nm correspond to optical transitions in GaN and InGaN, respectively. The average indium composition in the InGaN core region is estimated to be ~30%, if assuming the InGaN nanowires are fully relaxed.[29] The InGaN emission peak is relatively broad with a full width at half-maximum (fwhm) ~90 nm due to In phase separation. Schematically shown in Figure 1d, the InGaN/GaN nanowire structures can effectively function as a double-band photoelectrode.

Structural properties of the InGaN nanowires were further analyzed by scanning transmission electron microscopy (STEM) and energy dispersive X-ray spectrometry spectrum imaging (EDXS-SI), which were taken on a JEOL 2200FS transmission electron microscope operating at 200 kV. Figure 2a shows a high-angle annular dark field (HAADF) image of two InGaN nanowires, illustrating the atomic number contrast between GaN (darker) and InGaN (brighter) regions and also suggesting the core−shell structure for the nanowire. The nanowires are tapered with the diameter increasing from the bottom to top. As can be seen, the nanowires consist of three segments of InGaN (each ~70 nm long). The elemental distribution in the nanowire was analyzed by EDXS. Variations of the In Lα, Ga Kα, and N Kα signals along the nanowire axial direction (blue line in panel a) are plotted in Figure 2b, clearly showing the three InGaN segments. The EDXS line scans along the lateral direction (green lines in panel a) are shown in Figure 2c−e, which further confirms the InGaN (core)−GaN (shell) structure. It is also important to notice that the GaN shell is very thin and is estimated to be less than ~10, 15, and 20 nm for the top (line 2), middle (line 3), and bottom (line 4) segments, respectively. The formation of InGaN(core)/GaN(shell) structure is attributed to the enhanced surface desorption of In at the growth temperature and the difference in formation enthalpies between InN and GaN. At the growth temperature (~600 °C), the surface desorption of In atoms is significant, compared to Ga atoms. Because of the shadowing effect of the surrounding nanowires, impinged In flux may not readily arrive at the lateral surfaces of the nanowires to compensate for the desorbed In atoms during the MBE growth process. Consequently, a Ga-rich shell is formed spontaneously during the growth process. The GaN shell thickness can be controlled by the growth temperature and the thickness of InGaN segment and can be further varied by interrupting the In flux. In this work, the use of a relatively thin GaN shell can protect the InGaN core from photocorrosion without severely affecting the carrier transport. On the other hand, the tapered nanowire morphology is directly related to the enhanced lateral growth due to the reduced substrate temperature and enhanced indium incorporation.

Photoelectrochemical properties of InGaN/GaN nanowires were investigated using a cell with three-electrode configuration, which consists of an Ag/AgCl reference electrode, a Pt counter electrode, and an InGaN nanowire working electrode. A Wavenow electrochemical station (Pine Instrument Inc.) was used throughout this study. An alloy of Ga−In eutectic (Sigma-Aldrich) was deposited on the Si backside to make ohmic contact, which was subsequently connected with a Cu wire using

dx.doi.org/10.1021/nl402156e | Nano Lett. 2013, 13, 4356−4361

silver paste. The entire sample except the nanowire surface was then covered by insulating epoxy to eliminate any current leakage. All photoelectrochemical measurements were conducted in 1 mol/L HBr. The photoelectrochemical cell was evacuated after pouring the electrolyte solution into the reactor. A 300 W xenon arc lamp with either a 375 nm long-pass filter or an AM1.5G filter was used as the light source. The nanowire working electrode was illuminated through a quartz window. Sampling was done using a gastight syringe and was immediately analyzed by a gas chromatographer (Shimadzu GC-8A).

Figure 3a shows the measured current density as a function of applied potential for the InGaN nanowire photoanode under both dark and illumination conditions. The potential sweep rate was 20 mV/s. The bias was applied to the n-type InGaN working photoelectrode versus the Pt counter electrode and measured from the Ag/AgCl reference electrode. It is seen that the dark current is essentially negligible (~5 μA/cm^2, or less) even at high potentials of 1.0 V versus Ag/AgCl. To confirm the photoresponse of the InGaN core, measurements were performed with the use of a 375 nm long-pass filter, which prevented the excitation of the GaN shell region. Shown in Figure 3a, the photocurrent increases significantly with bias voltage and reaches ~11 mA/cm^2 at 1 V. When an AM1.5G filter is used, the photocurrent is significantly enhanced, which includes contributions from both the GaN shell and InGaN core regions. At 1 V, the measured current density is ~23 A/cm^2. These measured values are significantly higher than previously reported ones[32,37] due to the nearly defect-free core/shell structures and the superior charge carrier transport properties. In addition, the upward surface band bending due to the n-type characteristics of the nanowire structures, can further enhance charge separation and promote the transfer of holes to the nanowire surfaces for water oxidization reaction.[38,39] Detailed studies also confirm that the underlying Si substrate has negligible contribution to the measured photocurrent (see Supporting Information).

To further investigate the wavelength-dependent photoelectrochemical properties of InGaN nanowires and to derive the IPCE values, we have performed current−voltage measurements with the use of different band-pass optical filters (see Supporting Information). The IPCE describes the ratio of photogenerated electrons collected by the electrodes over the number of incident monochromatic photons. It can be calculated by the following equation

$$\mathrm{IPCE\%} = \frac{c \times h}{e} \frac{J(\mathrm{A\cdot cm^{-2}})}{\lambda(\mathrm{nm}) \times P(\mathrm{W\cdot cm^{-2}})} \times 100$$

where J is the photocurrent density, P is the incident radiation intensity at a given wavelength, λ is wavelength of the incident photon, and c, h, and e are the speed of light, the Planck constant, and the elementary electric charge, respectively. Shown in Figure 3b, at 1 V vs Ag/AgCl the maximum IPCE measured is 27.6% at 350 nm where both GaN and InGaN are activated. At 380 nm where only InGaN is excited, the IPCE value is 15.7%. Clear photoresponse was measured up to ~532 nm, which is in quantitative agreement with the PL emission peak (~522 nm) from the InGaN core region. The increasing IPCE with decreasing wavelength is largely related to the spectral absorbance of the InGaN,[40] schematically shown in Figure 3b. Additionally, carrier localization in indium-rich nanoclusters may contribute to the measured low efficiency in the long-wavelength range. In this regard, further improvement in the IPCE can be achieved by increasing the thickness of InGaN segments and by bandgap engineering. For example, incorporating different In compositions in each InGaN segment can lead to triple or even quadruple-band nanowire photoelectrodes with further enhanced efficiency. It is also important to note that due to the limited surface coverage (fill factor ~50%) the internal quantum efficiency of such structures is obviously higher than the values shown in Figure 3b.

Because of variations of the surface charge properties in harsh photocatalysis reactions, the chemical stability to anodic photooxidation has been a major concern for previously reported nanostructured photoelectrodes.[15,41] To examine the stability of InGaN/GaN nanowires, the sample was illuminated in 1 mol/L HBr solution over an extended period of time. Figure 4 shows

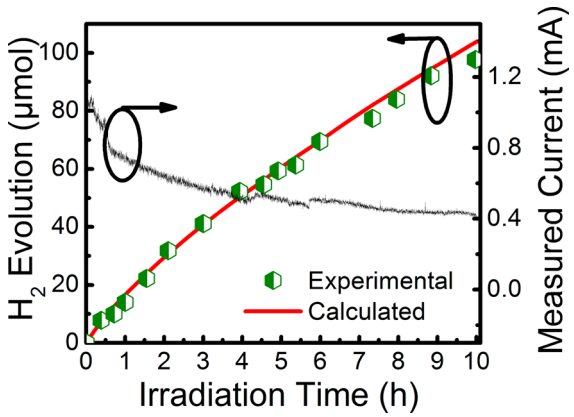

Figure 4. Steady H_2 evolution in 1 mol/L HBr at 0.2 V vs the counter electrode using a long-pass filter (>375 nm) in the two-electrode configuration. The H_2 evolution is also calculated from the measured current (solid red curve).

chronoamperometric experimental results along with H_2 gas evolution at a constant applied potential of 0.2 V vs the counter electrode with a 375 nm long-pass filter for a period of 10 h. Since InGaN band edges can straddle the oxidation and reduction potentials of water, an external bias theoretically is not required to split water. In this experiment, a small bias, that is, 0.2 V is applied to help overcome external losses, including the unoptimized resistive loss of the system. The measured photocurrent density is nearly steady. The relatively large photocurrent also leads to the direct observation of solar-to-hydrogen conversion. The evolved H_2 gas from the Pt counter electrode over time is shown in Figure 4. The gas production rate is directly proportional to the photocurrent density. Utilizing Faraday's law, the calculated H_2 gas generation from the measured photocurrent is also shown in Figure 4, which is in excellent agreement with the measured H_2. It was further observed that with increasing bias potential, the H_2 gas generation rate is significantly increased. Additionally, higher H_2 production rate was observed when an AM1.5G filter was utilized, due to contributions from the GaN region (see Supporting Information).

Finally, to further study the long-term stability of InGaN/GaN nanowires, their structural properties were thoroughly investigated using SEM, STEM, and EDXS-SI after 24 h chronoamperometric measurements in 1 mol/L HBr electrolyte (see Supporting Information). Figure 5a shows the HAADF image, suggesting the unchanged nanowire structure. The elemental distribution was further analyzed by EDXS. Variations of the In Lα, Ga Kα, and N Kα signals along the lateral direction

dx.doi.org/10.1021/nl402156e | Nano Lett. 2013, 13, 4356−4361

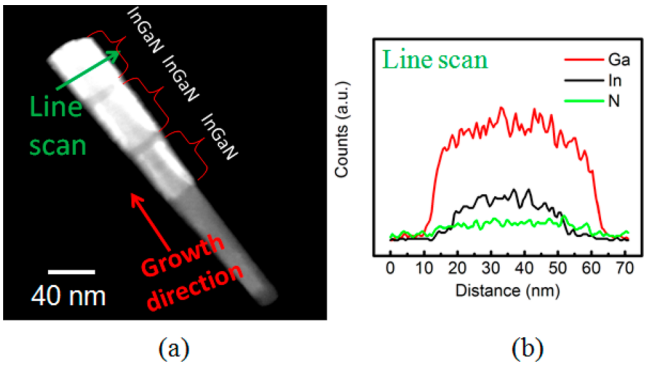

Figure 5. (a) High-angle annular dark-field image of InGaN/GaN nanowire after 24 h photoelectrochemical reaction in 1 mol/L HBr at a bias of 0.2 V vs the counter electrode. (b) Energy dispersive X-ray (EDX) line scan along the line shown in (a).

of the top segment (green line in Figure 5a) of the nanowire are shown in Figure 5b, which is nearly identical to the as-grown nanowire structures, illustrated in Figure 2. More detailed analysis further provides unambiguous evidence that there is no any degradation after 24 h photoelectrochemical reaction (see Supporting Information). This clearly demonstrates the stability of InGaN/GaN nanowires and its excellent resistance to photo-oxidation and corrosion. Previous work has shown that GaN is stable against photocorrosion.[32,42,43] In this study, the stability of n-type InGaN/GaN nanowire structures is attributed to the bunching of the surface states due to the strongly ionic bonds of III-nitride semiconductors.[33,34] The surface states are largely positioned near the band edges and do not serve as nonradiative recombination centers, which is consistent with the absence of surface Fermi level pinning measured on the grown surfaces of III-nitride nanowires.[44,45] Consequently, the surface states of GaN semiconductors may not contribute to surface oxidization, thereby leading to long-term stability against corrosion. The stability of InGaN/GaN nanowire photoanode is also partly attributed to the controlled surface polarity and the presence of negligible dislocations due to the effective lateral stress relaxation and the absence of epitaxial relationship between GaN nanowire and the underlying substrate.[46]

In summary, we have investigated the photoelectrochemical properties of double-band InGaN/GaN core/shell nanowire photoanodes, which can lead to stable hydrogen production under UV and visible light irradiation. The realization of a highly stable, scalable, and efficient photoanode in acidic solution addresses the critical need for future photoelectrochemical water splitting systems. It is also important to notice that such nanowire arrays are grown directly on low cost, large area Si substrate, providing the unique opportunity for integration with Si photocathode for developing high performance, low cost multijunction solar fuel systems.

■ ASSOCIATED CONTENT

Ⓢ Supporting Information

Additional information and figures. This material is available free of charge via the Internet at http://pubs.acs.org.

■ AUTHOR INFORMATION

Corresponding Author

*E-mail: zetian.mi@mcgill.ca. Phone: 1 514 398 7114.

Notes

The authors declare no competing financial interest.

■ ACKNOWLEDGMENTS

The authors wish to thank Dr. M. Harati for his help with the photoelectrochemical setup. This work is being supported by the Natural Sciences and Engineering Research Council of Canada (NSERC), the Fonds de recherché sur la nature et les technologies, and McGill University. Part of the work was performed in the McGill University Micro Fabrication Facility. Electron microscopy images and analysis was carried out at National research Council (NRC) Canada. B. AlOtaibi acknowledges King Abdullah foreign scholarship program.

■ REFERENCES

(1) Ciamician, G. *Science* **1912**, *36* (926), 385−394.
(2) Fujishima, A.; Honda, K. *Nature* **1972**, *238* (5358), 37−38.
(3) Borgarello, E.; Kiwi, J.; Pelizzetti, E.; Visca, M.; Gratzel, M. *Nature* **1981**, *289* (5794), 158−160.
(4) Khaselev, O.; Turner, J. A. *Science* **1998**, *280* (5362), 425−427.
(5) Gratzel, M. *Nature* **2001**, *414* (6861), 338−344.
(6) Maeda, K.; Domen, K. *J. Phys. Chem. Lett.* **2010**, *1* (18), 2655−2661.
(7) Turner, J. A. *Science* **1999**, *285* (5428), 687−689.
(8) Joshi, U. A.; Palasyuk, A.; Arney, D.; Maggard, P. A. *J. Phys. Chem. Lett.* **2010**, *1* (18), 2719−2726.
(9) Trammell, S. A.; Dressick, W. J.; Melde, B. J.; Moore, M. *J. Phys. Chem. C* **2011**, *115* (27), 13446−13461.
(10) Heller, A.; Aharonshalom, E.; Bonner, W. A.; Miller, B. *J. Am. Chem. Soc.* **1982**, *104* (25), 6942−6948.
(11) Boettcher, S. W.; Spurgeon, J. M.; Putnam, M. C.; Warren, E. L.; Turner-Evans, D. B.; Kelzenberg, M. D.; Maiolo, J. R.; Atwater, H. A.; Lewis, N. S. *Science* **2010**, *327* (5962), 185−187.
(12) Khan, S. U. M.; Akikusa, J. *J. Phys. Chem. B* **1999**, *103* (34), 7184−7189.
(13) Santato, C.; Ulmann, M.; Augustynski, J. *J. Phys. Chem. B* **2001**, *105* (5), 936−940.
(14) Sayama, K.; Nomura, A.; Zou, Z. G.; Abe, R.; Abe, Y.; Arakawa, H. *Chem. Commun.* **2003**, *23*, 2908−2909.
(15) Su, J. Z.; Guo, L. J.; Bao, N. Z.; Grimes, C. A. *Nano Lett.* **2011**, *11* (5), 1928−1933.
(16) Brillet, J.; Gratzel, M.; Sivula, K. *Nano Lett.* **2010**, *10* (10), 4155−4160.
(17) Yoshimura, J.; Ebina, Y.; Kondo, J.; Domen, K.; Tanaka, A. *J. Phys. Chem* **1993**, *97* (9), 1970−1973.
(18) Chen, X. B.; Liu, L.; Yu, P. Y.; Mao, S. S. *Science* **2011**, *331* (6018), 746−750.
(19) Ma, T. L.; Akiyama, M.; Abe, E.; Imai, I. *Nano Lett.* **2005**, *5* (12), 2543−2547.
(20) Hoang, S.; Guo, S. W.; Hahn, N. T.; Bard, A. J.; Mullins, C. B. *Nano Lett.* **2012**, *12* (1), 26−32.
(21) Lewis, N. S. *Inorg. Chem.* **2005**, *44* (20), 6900−6911.
(22) Chen, Y. W.; Prange, J. D.; Duhnen, S.; Park, Y.; Gunji, M.; Chidsey, C. E. D.; McIntyre, P. C. *Nat. Mater.* **2011**, *10* (7), 539−544.
(23) Rocheleau, R. E.; Miller, E. L.; Misra, A. *Energy Fuels* **1998**, *12* (1), 3−10.
(24) Khaselev, O.; Bansal, A.; Turner, J. A. *Int. J. Hydrogen Energy* **2001**, *26* (2), 127−132.
(25) Fujii, K.; Karasawa, T. K.; Ohkawa, K. *Jpn J. Appl. Phys. 2* **2005**, *44* (16−19), L543−L545.
(26) Fujii, K.; Ohkawa, K. *Jpn. J. Appl. Phys., Part 2* **2005**, *44* (28−32), L909−L911.
(27) Theuwis, A.; Strubbe, K.; Depestel, L. M.; Gomes, W. P. *J. Electrochem. Soc.* **2002**, *149* (5), E173−E178.
(28) Wu, J. Q. *J. Appl. Phys.* **2009**, *106* (1), 011101.
(29) Moses, P. G.; Van de Walle, C. G. *Appl. Phys. Lett.* **2010**, *96* (2), 021908.
(30) Wang, D. F.; Pierre, A.; Kibria, M. G.; Cui, K.; Han, X. G.; Bevan, K. H.; Guo, H.; Paradis, S.; Hakima, A. R.; Mi, Z. T. *Nano Lett.* **2011**, *11* (6), 2353−2357.

(31) Fujii, K.; Kusakabe, K.; Ohkawa, K. *Jpn J. Appl. Phys., Part 1* **2005**, *44* (10), 7433−7435.
(32) Luo, W. J.; Liu, B.; Li, Z. S.; Xie, Z. L.; Chen, D. J.; Zou, Z. G.; Zhang, R. *Appl. Phys. Lett.* **2008**, *92* (26), 262110.
(33) Foresi, J. S.; Moustakas, T. D. *Appl. Phys. Lett.* **1993**, *62* (22), 2859−2861.
(34) Moustakas, T. D. *Phys. Status Solidi A* **2013**, *210* (1), 169−174.
(35) Chang, Y. L.; Wang, J. L.; Li, F.; Mi, Z. *Appl. Phys. Lett.* **2010**, *96* (1), 013106.
(36) Nguyen, H. P. T.; Zhang, S.; Cui, K.; Han, X.; Fathololoumi, S.; Couillard, M.; Botton, G. A.; Mi, Z. *Nano Lett.* **2011**, *11* (5), 1919−1924.
(37) Hwang, Y. J.; Wu, C. H.; Hahn, C.; Jeong, H. E.; Yang, P. D. *Nano Lett.* **2012**, *12* (3), 1678−1682.
(38) Wallys, J.; Hoffmann, S.; Furtmayr, F.; Teubert, J.; Eickhoff, M. *Nanotechnology* **2012**, *23* (16), 165701.
(39) AlOtaibi, B.; Harati, M.; Fan, S.; Zhao, S.; Nguyen, H. P. T.; Kibria, M. G.; Mi, Z. *Nanotechnology* **2013**, *24* (17), 175401.
(40) Hahn, C.; Zhang, Z. Y.; Fu, A.; Wu, C. H.; Hwang, Y. J.; Gargas, D. J.; Yang, P. D. *ACS Nano* **2011**, *5* (5), 3970−3976.
(41) Kay, A.; Cesar, I.; Gratzel, M. *J. Am. Chem. Soc.* **2006**, *128* (49), 15714−15721.
(42) Huygens, I. M.; Strubbe, K.; Gomes, W. P. *J. Electrochem. Soc.* **2000**, *147* (5), 1797−1802.
(43) Aryal, K.; Pantha, B. N.; Li, J.; Lin, J. Y.; Jiang, H. X. *Appl. Phys. Lett.* **2010**, *96* (5), 052110.
(44) Wu, C. L.; Lee, H. M.; Kuo, C. T.; Chen, C. H.; Gwo, S. *Phys. Rev. Lett.* **2008**, *101* (10), 106803.
(45) Zhao, S.; Fathololoumi, S.; Bevan, K. H.; Liu, D. P.; Kibria, M. G.; Li, Q.; Wang, G. T.; Guo, H.; Mi, Z. *Nano Lett.* **2012**, *12* (6), 2877−2882.
(46) Zhao, S.; Kibria, M. G.; Wang, Q.; Nguyen, H. P. T.; Mi, Z. *Nanoscale* **2013**, *5* (12), 5283−5287.